Asian Journal of Chemistry; Vol. 36, No. 11 (2024), 2521-2529

ASIAN JOURNAL OF CHEMISTRY

https://doi.org/10.14233/ajchem.2024.32292

Inhibitory Potential of N-Methyl Formanilide on Mild Steel Corrosion in Sulfuric Acid: Quantum Chemical and Experimental Perspectives

MEENAKSHI GUPTA[1], NEETA AZAD[1], MANSI Y. CHAUDHARY[2], YUDHVIR S. SHARMA[2] and SHRAMILA YADAV[2,*]

[1]Department of Chemistry, Atma Ram Sanatan Dharma College, University of Delhi, New Delhi-110010, India
[2]Department of Chemistry, Rajdhani College, University of Delhi, New Delhi-110015, India

*Corresponding author: E-mail: syadav@rajdhani.du.ac.in

Received: 16 August 2024; *Accepted*: 8 October 2024; *Published online*: 30 October 2024; AJC-21785

Technological progress has led to increased use of metals and alloys such as aluminum, brass, bronze and mild steel. While mild steel is favoured for its availability, low cost and excellent mechanical properties, it is prone to corrosion. This study aims to reduce the corrosion of mild steel in sulfuric acid using N-methyl formanilide (NMF) as an inhibitor. The effectiveness of NMF was evaluated using gravimetric method (weight loss) and electrochemical impedance spectroscopy (EIS). Surface analyses were conducted using atomic force microscopy (AFM) and scanning electron microscopy (SEM). The study examined the performance of NMF at different temperatures (298 K to 338 K) and varying inhibitor concentrations. The results indicated that the percentage inhibition efficiency (%IE) of NMF increased with higher concentration but decreased with temperature. The NMF formed a protective layer on mild steel through physical adsorption, which was confirmed by El-Awady adsorption isotherm and comparing it with other adsorption models. The kinetic and thermodynamic studies were also performed, with activation energy (E_a) and adsorption free energy (ΔG°_{ads}) being calculated. These findings were further validated using the AM1 quantum mechanical method, revealing the promising results for the investigation.

Keywords: Adsorption, Gravimetric method, N-Methyl formanilide, Quantum chemical studies, El-Awady adsorption isotherm.

INTRODUCTION

Sulfuric acid is the largest used chemical in metal pickling, petroleum purification, acidizing in the gas and oil industry, fertilizer production, oil-well vacuuming, electroplating of metal, *etc.* nonetheless it is highly corrosive [1-4]. Thus, it is a source of corrosion of metal containers in industry and lowers their life period. Therefore, the corrosion inhibitors are employed in acids to mitigate their corrosive effects on metals and reduce financial losses to the industry. Corrosion also depends on the pH of the solution [5,6] *i.e.* at low pH, corrosion is more due to high hydrogen evolution and greater accessibility of oxygen to the metal surface. Usually, there is a formation of oxide diffusion barrier film on the peripheral of iron at a pH below 4 [7-9].

The organic compounds that contain heteroatoms such as oxygen, nitrogen, sulfur and phosphorus or those with conjugated systems, are often identified as effective inhibitors [10-14]. This efficacy is attributed to their free electrons, which can form bonds with the metal surfaces. An organic inhibitor's performance depends on its ability to adsorb onto the metal surface, creating a protective layer or reducing the rate at which reactants diffuse across the metal [15,16]. The electrolyte aggression, inhibitor molecule structure, charge distribution and metal surface charge play important roles in the adsorption process [17-21]. Corrosion inhibitors typically include compounds with an extended π-e^- system, long chains and functional groups, such as -NR_2, -C=C-, -NH_2, -$CONH_2$, -SR, -COOH, -OH and -OR, since such groups typically have an electron available to bind with the metal and be adsorbed [22-25]. These structural components actively reduce corrosion rates by improving the protective capacities of metal atoms through donor-acceptor (D-A) interactions. This approach not only helps preserve the integrity of materials but also contributes to longer service life and lower maintenance costs [26].

Several researchers have highlighted the corrosion inhibition potential of conjugated 4-aminoantipyrine-based Schiff bases [27], polyaniline (PANI), poly(*N*-methylaniline) (PNMA)

and poly-(*N*-formylanilide) (PNFA) coatings [28] and 3-nitro-5-(2-amino-1,3,4-thiadiazolyl)nitrobenzene (NATN) [29], *etc*. The presence of heteroatoms and conjugation makes these compounds promising candidates for corrosion protection applications. Recently, Wang *et al.* [30] evaluated the effectiveness of six nitrogen-containing organic compounds as copper corrosion inhibitors in H_2O_2 and sarcosine (SAR) alkaline medium. Similarly, subphthalocyanine chloride (SubPc) [31] and 5,5-diphenyl-3,5-dihydro-4*H*-imidazol-4-one (AM6) [32] have also been evaluated as a green corrosion inhibitor for mild steel in acidic environments. These findings highlighted the varying effectiveness of different nitrogen-containing compounds in mitigating corrosion under specific conditions.

Thus, in this investigation, N-methylformanilide (NMF) which contains heteroatom nitrogen, oxygen, electron-donating methyl group and π-electrons is used to inhibit the mild steel corrosion in 0.5 mol/L sulfuric acid. Moreover, NMF is indeed considered as non-toxic when inhaled, making it a safer option in various applications including as a swelling agent and precursor for numerous chemical compounds. This combination of safety and functionality enhances its potential as a corrosion inhibitor.

EXPERIMENTAL

The corrosion behaviour of mild steel in N-methylformanilide (NMF) sulfuric acid solution was investigated using various methods including weight loss measurements, electrochemical impedance spectroscopy (EIS), atomic force microscopy (AFM), scanning electron microscopy (SEM) and chemical quantum studies (CQS).

Specimen preparation: For weight loss studies, mild steel coupons measuring 1 cm × 1 cm × 1 cm were employed, while for electrochemical impedance spectroscopy (EIS), mild steel samples with a bare area of 1 cm^2 were used. Surface analysis was conducted on specimens sized 1 cm × 1 cm × 0.5 cm. The mild steel surfaces were polished to a glass-like finish using emery papers ranging from 100 to 1200 grit, then thoroughly cleaned with solvents (distilled water and acetone) and dried at room temperature. The EIS measurements were carried out using a three-electrode setup consisting of platinum, calomel and mild steel electrodes.

Inhibitor solution: Different concentrations of NMF *i.e.* 10^{-1} M, 10^{-3} M, 10^{-5} M and 10^{-7} M were prepared in 0.5 mol/L sulfuric acid to assess the corrosion action of mild steel in these solutions [33].

Weight loss studies: Varying concentrations (10^{-1} M, 10^{-3} M, 10^{-5} M and 10^{-7} M) of inhibitor NMF in 0.5 mol/L H_2SO_4 were prepared and the specimens were dipped in these solutions at different temperatures (298 K, 308 K, 318 K and 328 K) for 6 h to perform the weight loss evaluations. After 6 h, the mild steel coupons were washed with double distilled water to remove all the corrosive materials properly then dried in a desiccator for 24 h. They were subsequently weighed to determine the total weight loss for each coupon and further parameters were then calculated.

Electrochemical impedance studies (EIS): The EIS experiment was conducted at 298 K by immersing mild steel in 10^{-1} M NMF solution and an acid solution for 6 h. The parameters of EIS including charge transfer resistance (R_{ct}) and double-layer capacitance (C_{dl}) were evaluated from the Nyquist plot [34].

Thermodynamic adsorption studies: Thermodynamics *i.e.* change in temperature plays a vital role in the inhibition of corrosion by affecting the interaction between metal and acidic medium [35]. It is apparent from the thermodynamic calculation that NMF follows El-Awady adsorption isotherm for mild steel in sulfuric acid and the adsorption parameters like equilibrium constant (K_{ads}), standard Gibb's free energy (ΔG°_{ads}) and activation energy (E_a) were calculated and analyzed using weight loss data [34,36].

Surface morphology studies: Polished mild steel coupons (1 cm × 1 cm × 0.5 cm) were dipped in 0.5 mol/L H_2SO_4, in 10^{-1} M and 10^{-7} M of NMF solution at 298 K for 24 h to study the surface morphology of mild steel and then subjected to a JEOL 840 JSM scanning electron microscope for SEM studies. The AFM images were obtained from VEECO CPII microscope instrument.

Quantum studies: The chemical structure of NMF was generated using Hyperchem 7.5 software. Initially, the structure was optimized using the MM+ (Molecular Mechanics) method, followed by re-optimization with the AM1 method utilizing the Polak-Ribière gradient approach. The optimization was performed with a convergence threshold of 0.01 kcal/mol/Å for total energy. Various parameters, including the highest occupied molecular orbital energy (E_{HOMO}), the lowest unoccupied molecular orbital energy (E_{LUMO}), the energy gap (ΔE), binding energy and dipole moment were calculated.

RESULTS AND DISCUSSION

Weight loss measurements: Gravimetric method was used to calculate the inhibition efficiency (IE) and corrosion rate (C_r) of mild steel using eqns. 1 and 2, respectively [37,38]:

$$IE\ (\%) = \left(1 - \frac{w_i}{w_o}\right) \times 100 \quad (1)$$

where w_o represents the weight lost by mild steel in acid solution and w_i denotes the weight lost by mild steel in inhibitor solution.

$$C_r = \frac{kW_L}{At\rho} \quad (2)$$

where C_r represents the corrosion rate of the mild steel in mm/year; k is constant with a value of 87.6; W_L is the weight loss of mild steel in mg; and t is the immersion time in hours (6 h for performing experiment); ρ is the density of mild steel (7.06 g/cm^3) and A refers to the area of mild steel specimen (1 cm^2).

The calculated values for IE and C_r are summarized in Table-1. The graph of IE *versus* the logarithm of inhibitor concentration (Fig. 1) at various temperatures demonstrates that IE % decreases with increasing temperature across all inhibitor concentrations, while it increases with higher inhibitor concentrations. The corrosion rate is higher in the uninhibited solution compared to the inhibited solutions at all temperatures indicating that mild steel experiences the minimal corrosion in the NMF solution.

TABLE-1
WEIGHT LOSS DATA FOR MILD STEEL IN 0.5 mol/L H_2SO_4 CONTAINING NMF

Temp. (K)	Conc. (M)	Initial weight I_w (g)	Final weight F_w (g)	Weight loss (g)	IE (%)	C_r (mm/y)
298	10^{-1}	6.8944	6.8811	0.0133	83.1	27.50425
	10^{-3}	7.1045	7.0873	0.0172	78.2	35.56941
	10^{-5}	7.9630	7.9436	0.0194	75.4	40.11898
	10^{-7}	6.7546	6.7349	0.0197	75.0	40.73938
	Acid	7.4629	7.3841	0.0788	–	162.9575
308	10^{-1}	6.5125	6.4946	0.0179	79.1	37.0170
	10^{-3}	6.1893	6.1689	0.0204	76.1	42.18697
	10^{-5}	7.6403	7.6127	0.0276	67.7	57.07649
	10^{-7}	7.4536	7.4183	0.0353	58.7	73.0000
	Acid	7.3616	7.2761	0.0855	–	176.8130
318	10^{-1}	6.9462	6.8782	0.068	73.8	140.6232
	10^{-3}	6.5048	6.4303	0.0745	71.3	154.0652
	10^{-5}	6.8241	6.7189	0.1052	59.4	217.5524
	10^{-7}	6.9626	6.8303	0.1323	49.0	273.5949
	Acid	7.0705	6.8113	0.2592	–	536.0227
328	10^{-1}	7.4696	7.3818	0.0878	71.10	181.5694
	10^{-3}	7.5032	7.4104	0.0928	69.40	191.9093
	10^{-5}	5.9706	5.8308	0.1398	54.00	289.1048
	10^{-7}	6.3974	6.2398	0.1576	48.10	325.9150
	Acid	7.6199	7.3162	0.3037	–	628.0482

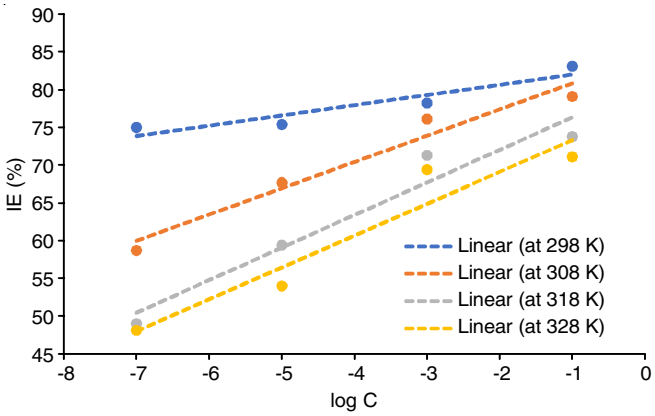

Fig. 1. Variation of IE with NMF concentration

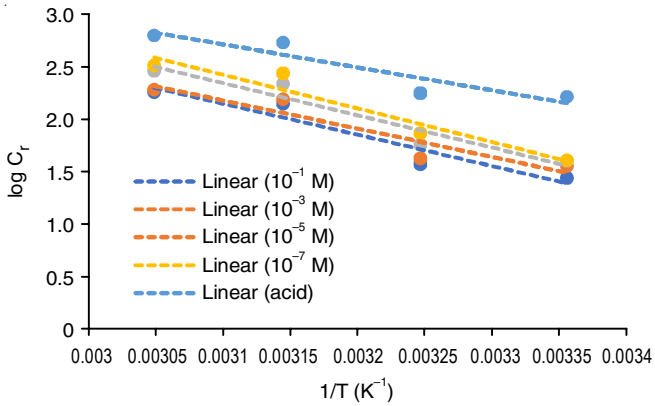

Fig. 2. log C_r *vs.* 1/T for different concentrations of NMF

Effect of temperature: The weight loss measurements were conducted at different temperatures (ranging from 298 K to 328 K) in both the absence and presence of NMF in 0.5 mol/L H_2SO_4. It was observed that the corrosion rates of mild steel increased with rising temperatures, both in the uninhibited and inhibited acid solutions. The relationship between the corrosion rate and temperature can be described using the Arrhenius equation (eqn. 3) [39,40]:

$$k = Ae^{-E_a/RT} = C_r \quad (3)$$

where k is the rate constant, A is the pre-exponential factor, E_a is the activation energy, R is the universal gas constant and T is the absolute temperature. The plot of log C_r *versus* 1/T for different concentrations of NMF yields a straight line (Fig. 2). The slope of this line is used to estimate the activation energy (E_a) by eqn. 3.

The activation energy in the presence of NMF, at all concentrations is higher compared to that in the acid solution alone, indicating that NMF effectively inhibits corrosion (Table-2). An activation energy value below 80 kJ/mol suggests physisorption and based on the data, it is evident that NMF adsorbs onto the mild steel surface through weak van der Waals forces (physisorption) [41].

TABLE-2
ENERGY OF ACTIVATION (E_a) OF CORROSION OF MILD STEEL IN THE ABSENCE AND PRESENCE OF NMF

Conc. of NMF (mol L^{-1})	E_a (kJ mol^{-1})
0	41.84
10^{-1}	56.84
10^{-3}	51.56
10^{-5}	59.02
10^{-7}	61.61

Adsorption isotherm: The mechanism of corrosion inhibition of mild steel by the NMF molecule can be understood by analyzing various adsorption isotherms, including El-Awady, Frumkin, Temkin, Freundlich, Langmuir and Flory-Huggins isotherms. The degree of surface coverage (θ) values were calculated from the weight loss measurements using eqn. 4 [42]:

$$\theta = 1 - \frac{w_i}{w_o} \quad (4)$$

where w_i and w_o is weight loss of mild steel in inhibited and uninhibited solution respectively.

Fig. 3 shows a straight line in the plot of log θ/(1 – θ) *vs.* log C with a correlation coefficient of 0.9270. This linear relationship suggests that the adsorption of NMF on the mild steel surface in H_2SO_4 follows the El-Awady adsorption isotherm.

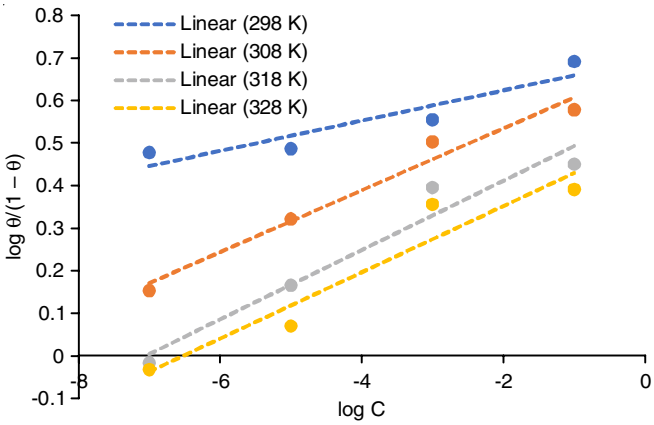

Fig. 3. El-Awady adsorption isotherms for NMF at different temperatures

El-Awady adsorption isotherm is given by eqn. 5:

$$\frac{\theta}{1-\theta} = K'C^{y}$$

$$\log\frac{\theta}{1-\theta} = \log K' + y\log C \quad (5)$$

A plot of log θ/1–θ *vs.* log C gives a straight line of slope y is no. of actives sites and the intercept is log K′ where adsorption equilibrium constant $K_{ads} = K'(1/y)$ [43-46]. If the 1/y value is less than one then multilayer adsorption by the inhibitor molecule and if the value is greater than one indicates the inhibitor occupies more than one active site [47]. From Table-3, it can be seen 1/y is more than unity so, NMF molecules occupies more than one active site.

The K_{ads} for the adsorption-desorption process was also determined at different temperatures and the values are reported in Table-3. Higher the K_{ads}, higher would be the adsorption ability of compound on the mild steel surface [48], thus from the present data it can be concluded that NMF molecules adsorbed effectively on mild steel surface. As temperature rises, the decrease in K_{ads} suggesting NMF adsorption capability on mild steel decreases with increasing temperature and so does inhibition efficiency. The Gibb's free energy of adsorption at different temperatures was calculated from the values of K_{ads} using eqn. 6:

$$\Delta G_{ads} = RT\ln(55.5K_{ads}) \quad (6)$$

The high and negative value of ΔG_{ads} (Table-3) reveals the spontaneity of adsorption of NMF on the surface of mild steel. The decrease in free energy of adsorption with an increase in temperature further supports the physical adsorption of NMF on the surface of mild steel [49,50].

Electrochemical impedance studies (EIS): EIS measurements were conducted on mild steel coupons immersed in both acid and inhibitor solutions. The resulting data were used to generate Nyquist and Bode plots (Fig. 4a-b). The charge transfer resistance (R_{ct}) was determined by measuring the diameter of the semi-circle in the Nyquist plot, while the double-layer capacitance (C_{dl}) was calculated using eqn. 7:

TABLE-3
ADSORPTION PARAMETERS OF MILD STEEL IN THE ABSENCE AND PRESENCE OF NMF

Temp. (K)	y	1/y	K′	R^2	K_{ads} (mol^{-1})	ΔG_{ads} (KJ mol^{-1})
298	0.0356	28.09	4.95	0.9599	3.31×10^{19}	-121.33
308	0.0729	13.72	4.80	0.9928	2.15×10^{9}	-65.32
318	0.0816	12.26	3.75	0.9937	1.10×10^{7}	-53.49
328	0.0779	12.84	3.21	0.9960	3.26×10^{6}	-51.86

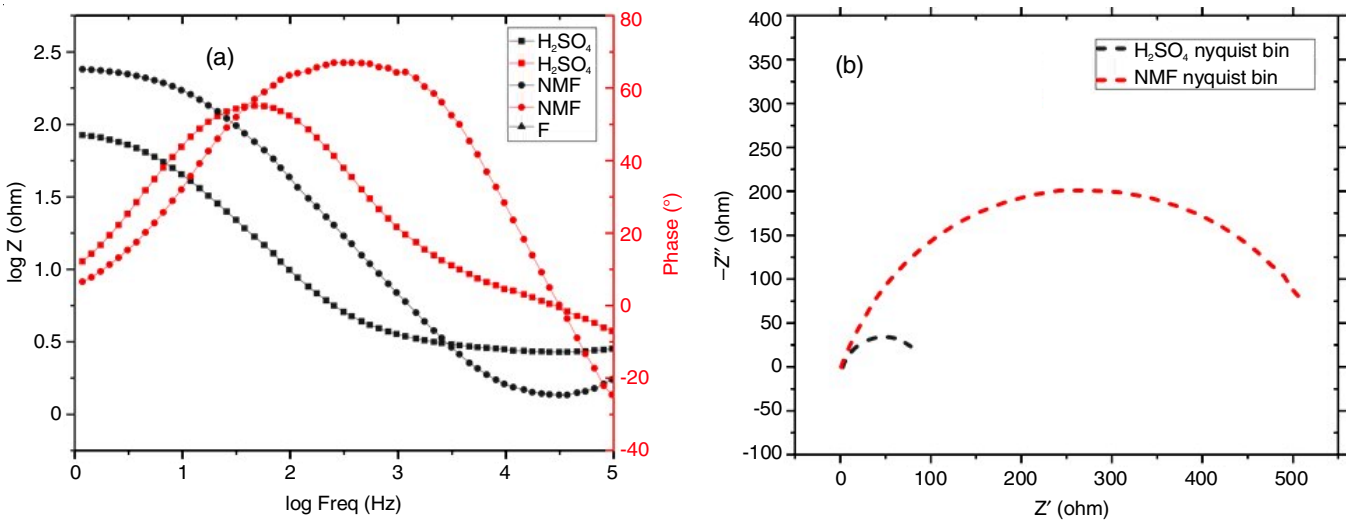

Fig. 4. (a) Bode plot for mild steel in 1 N H_2SO_4 and the presence of NMF at 298 K, (b) Nyquist plot for mild steel in 1 N H_2SO_4 and the presence of NMF at 298 K

$$C_{dl} = \frac{1}{(2\pi f R_{ct})} \quad (7)$$

The double-layer capacitance (C_{dl}) was calculated from the maximum frequency (f) at the peak of semi-circle in the imaginary component of Nyquist plot. The inhibition efficiency (IE) derived from EIS data is represented as follows:

$$IE = \frac{R_{ct(i)} - R_{ct(a)}}{R_{ct(i)}} \times 100 \quad (8)$$

where $R_{ct\,(i)}$ and $R_{ct\,(a)}$ are the charge transfer resistances in the presence of inhibitor and in the acid solutions, respectively. The larger diameter of the capacitive loop in the presence of NMF compared to the acid solution indicates that NMF effectively blocks the corrosion sites on mild steel, demonstrating its efficacy as a corrosion inhibitor [51]. The NMF enhances the value of R_{ct} and significantly reduces the C_{dl} value, suggesting that NMF molecules adsorb onto the mild steel surface and act as an effective inhibitor. The observed decrease in C_{dl} in the presence of inhibitor (Table-4) is attributed to the growth of electrical double layer, which signifies that NMF inhibits corrosion through adsorption.

TABLE-4
ELECTROCHEMICAL IMPEDANCE PARAMETERS

Compound	R_{ct} (Ω/cm^2)	f (Hz)	C_{dl} (F/cm^2)	IE (%)
NMF	550	9.98	2.9×10^{-5}	82.7
H_2SO_4	95	5.49	3.06×10^{-4}	–

SEM studies: Scanning electron microscopy (SEM) was used to analyze the changes in surface morphology or defects on mild steel exposed to both acidic and inhibitor solutions. Fig. 5a depicts a SEM image of a plain polished mild steel surface, which appears smooth with only minor abrasion marks whereas Fig. 5b illustrates the surface of mild steel after expo-

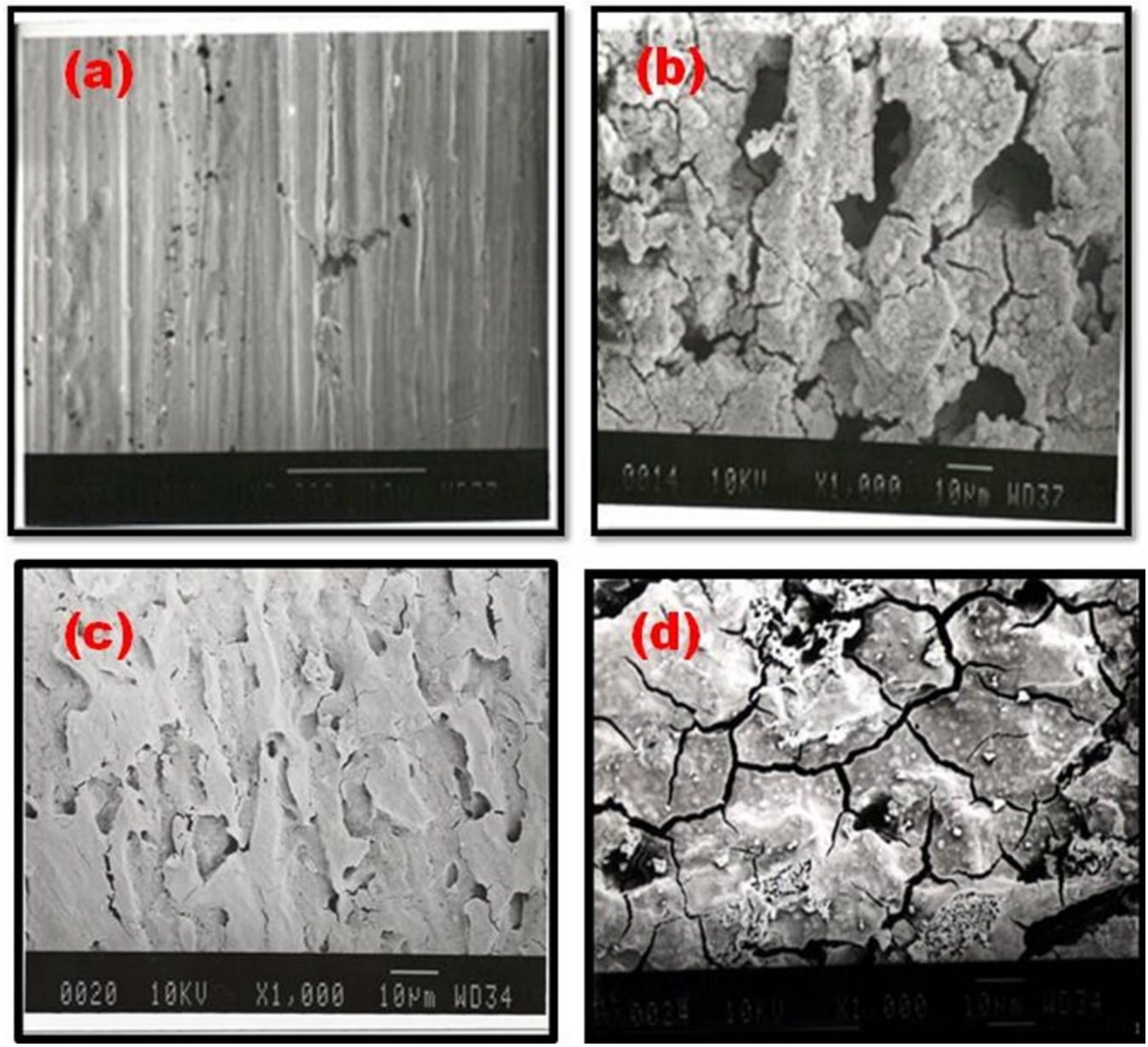

Fig. 5. Scanning electron micrographs of mild steel surfaces

sure to 0.5 mol/L sulfuric acid, showing a significant corrosion pits and surface damage, thereby confirming the corrosive effect of sulfuric acid on mild steel.

Fig. 5c-d display SEM images of mild steel surfaces treated with 10^{-1} M and 10^{-7} M NMF solutions, respectively. A smoother surface is observed in the presence of inhibitor (Fig. 5c), indicating that the inhibitor molecules create a protective layer that reduces mild steel dissolution in the corrosive medium [52,53]. On the other hand, Fig. 5d shows cracks and holes in this protective layer at lower inhibitor concentrations, which suggests that mild steel corrodes more at lower concentrations compared to higher ones. This implies that NMF inhibits mild steel corrosion in 0.5 mol/L sulfuric acid by neutralizing the acid, making the environment less corrosive. Moreover, NMF contributes to corrosion inhibition through electron donation from nitrogen and oxygen atoms and by existing as a protonated species that adsorbs onto the metal surface, forming a protective barrier against acid attack [54].

Atomic force microscopy (AFM): Fig. 6a-b display AFM micrographs of mild steel surfaces exposed to sulfuric acid and a 10^{-1} M NMF inhibitor solution, respectively. The AFM image of mild steel in sulfuric acid reveals deep pits and holes, whereas the image of mild steel in the NMF solution shows a smoother surface with a protective layer. Fig. 6b illustrates that the NMF forms a protective layer on the mild steel, with spherical particles gradually covering the surface, reducing corrosion. The effectiveness of the NMF inhibitor can be quantitatively verified by comparing the root mean square (RMS) roughness values, which reflect the surface roughness caused by corrosion [55]. A higher RMS value indicates greater surface roughness due to more extensive corrosion. The RMS values for mild steel in uninhibited and inhibited solutions are 176.5 nm and 25.1 nm, respectively. This significant reduction in the RMS value demonstrates that NMF effectively decreases surface roughness indicating its efficiency as a corrosion inhibitor.

Quantum chemical calculations: The quantum chemical parameters offer valuable insights into the relationship between molecular structure and inhibition efficiency (Fig. 7). From the optimized geometry of the inhibitor molecule in the gas phase, several parameters were calculated, including the highest

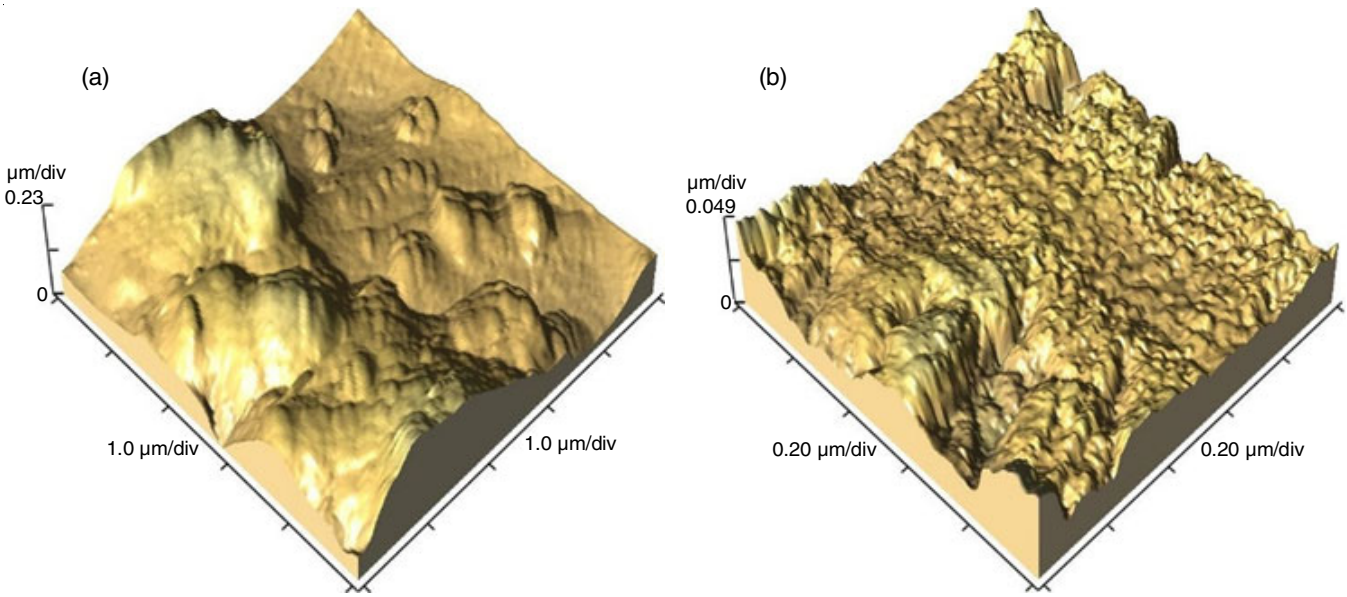

Fig. 6. Mild steel in acid (a) without NMF (b) with NMF

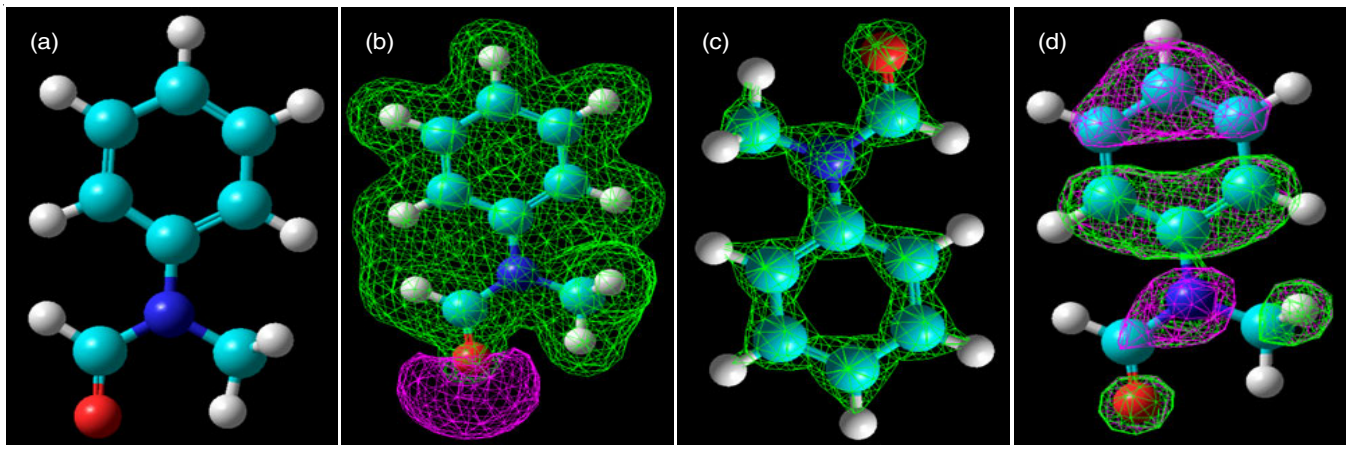

Fig. 7. (a) Optimized geometry of NMF (b) Charge distribution of NMF (c) Electrostatic Potential surface of NMF (d) 3D Isosurface of the total charge density on NMF HOMO and LUMO

TABLE-5
OPTIMIZED AM1 PARAMETERS FOR NMF

No. of electrons	E_{HOMO} (eV)	E_{LUMO} (eV)	Binding energy (Kcal/mol)	Dipole moment (Debyes)	$\Delta E = E_{LUMO} - E_{HOMO}$ (eV)
58	-8.823	0.4364	-2288.26	3.53	8.3866

TABLE-6
VARIOUS INHIBITORS HAVING COMPARATIVE EFFICIENCY WITH NMF

Name of inhibitor used	Environment	Inhibition efficiency	Adsorption mechanism	Ref.
(E)-N(2-Chlorobenzylidene)-2-fluorobenzenamine (NCF) and (E)-N(2-chlorobenzylidene)-3-chloro-2-methylbenzenamine (NCCM)	Carbon steel in 1 M HCl	NCF: 89.72% NCCM: 85.69%	Langmuir isotherm model	[56]
Aniline	Aluminum in 1.4 M HCl	Less than 30%	Langmuir isotherm model	[57]
3-(Imidazole[1,2-*a*]pyridine-2-yl)aniline-IPA	Mild Steel in HCl	59%	Langmuir isotherm model	[58]
2-Ethyl aniline and 2,4-dimethyl aniline	Steel in 15% HCl	2-Ethyl aniline: 78.3% 2,4-dimethyl aniline: 77.3%	Temkin adsorption isotherm	[59]
6-*Bis*(3,5-dimethyl-1*H*-pyrazol-1-yl)-N-phenyl-1,3,5-triazin-2-amine (**PTA-1**), N-(4-bromophenyl)-4,6-*bis*(3,5-dimethyl-1*H*-pyrazol-1-yl)-1,3,5-triazin-2-amine (**PTA-2**) and 4,6-*bis*(3,5-dimethyl-1*H*-pyrazol-1-yl)-N-(4-methoxyphenyl)-1,3,5-triazin-2-amine (**PTA-3**	Carbon steel in 0.25 M H_2SO_4	PTA-1: 18.6% PTA-2: 85.4% PTA-3: 84.5%	PTA-1: Frumkin adsorption isotherm, PTA-2: Langmuir adsorption isotherm, PTA-3: Langmuir adsorption isotherm	[60]
N-Ethyl N-hydroxyethyl aniline (NENHEA)	Mild steel in 0.5 M H_2SO_4	87.7%	Langmuir-Freundlisch adsorption isotherm	[61]
1,10-Phenanthroline, pyridine and quinoline	Mild steel	1,10-Phenanthroline: 80.4% Pyridine: 46.00% Quinoline: 64.00%	Modified Langmuir isotherm	[62]

occupied molecular orbital (HOMO), lowest unoccupied molecular orbital (LUMO), energy gap (ΔE), binding energy and dipole moment.

The calculated values for HOMO and LUMO, along with a lower energy gap, align with the experimental results showing that NMF is an effective corrosion inhibitor (Table-5). The negative binding energy indicates that the inhibitor molecules are stable, less likely to dissociate and provide substantial protection to the mild steel surface. Furthermore, a higher dipole moment suggests greater polarity, which enhances adsorption on mild steel and, consequently, improves inhibition efficiency. NMF shows strong polarity with a dipole moment of 3.53 Debye, so verifying its efficiency as a corrosion inhibitor.

Comparative analysis: Several studies have been noted that demonstrate comparable or lower inhibition efficiencies compared to N-methylformamide (NMF). Table-6 presents the data on various metals in different environments with reference to the achieved inhibitor's efficiencies.

Conclusion

Corrosion inhibitors for mild steel are widely used across various industries due to the metal susceptibility to rust and degradation. N-Methylformanilide (NMF) has been examined as a corrosion inhibitor for mild steel in sulfuric acid using electrochemical analysis and quantum chemical calculations across different concentrations and temperatures. These analyses confirmed that NMF effectively inhibits mild steel corrosion in sulfuric acid. The inhibition efficiency increases with NMF concentration but decreases with rising temperature. Thermodynamic studies indicate that NMF adsorbs physically onto the mild steel surface, as evidenced by an activation energy (E_a) value less than 80 kJ/mol and follows El-Awady adsorption iostherm. The increased activation energy in inhibitor solution signifies reduced corrosion. The EIS studies revealed more pronounced capacitive semicircle with NMF, indicating high inhibition efficiency. The SEM and AFM images demonstrate the formation of a protective layer on the mild steel surface, with AFM showing reduced surface roughness (RMS) in the presence of NMF, highlighting its effectiveness as a corrosion inhibitor. Moreover, the computational results for E_{HOMO}, E_{LUMO} and energy gap (ΔE) are well correlated with the observed corrosion inhibition efficiency.

CONFLICT OF INTEREST

The authors declare that there is no conflict of interests regarding the publication of this article.

REFERENCES

1. T.W. Quadri, L.O. Olasunkanmi, O.E. Fayemi, H. Lgaz, O. Dagdag, E.M. Sherif, A.A. Alrashdi, E.D. Akpan, H.S. Lee and E.E. Ebenso, *Arab. J. Chem.*, **15**, 103870 (2022); https://doi.org/10.1016/j.arabjc.2022.103870
2. M. Swathika, K.R.B. Singh, M. Mehala, S. Pandey, J. Singh, R.P. Singh and A. Natarajan, *RSC Adv.*, **12**, 14888 (2022); https://doi.org/10.1039/D2RA01773C
3. M. Goyal, H. Vashist, S. Kumar, I. Bahadur, F. Benhiba and A. Zarrouk, *J. Mol. Liq.*, **315**, 113705 (2020); https://doi.org/10.1016/j.molliq.2020.113705
4. C. Verma, L.O. Olasunkanmi, E.E. Ebenso and M.A. Quraishi, *Results Phys.*, **8**, 657 (2018); https://doi.org/10.1016/j.rinp.2018.01.008

5. X. Li, P. Zhang, H. Huang, X. Hu, Y. Zhou and F. Yan, *RSC Adv.*, **9**, 39055 (2019); https://doi.org/10.1039/C9RA08482G
6. C. Zea, R. Barranco-García, J. Alcántara, J. Simancas, M. Morcillo and D. de la Fuente, *Micropor. Mesopor. Mater.*, **255**, 166 (2018); https://doi.org/10.1016/j.micromeso.2017.07.035
7. G.M. Atenas, E. Mielczarski and J.A. Mielczarski, *J. Colloid Interface Sci.*, **289**, 157 (2005); https://doi.org/10.1016/j.jcis.2005.03.062
8. F.M. Song, D.W. Kirk, J.W. Graydon and D.E. Cormack, *Corrosion*, **58**, 145 (2002); https://doi.org/10.5006/1.3277315
9. H. Parangusan, J. Bhadra, and N. Al-Thani, *Emergent Mater.*, **4**, 1187 (2021); https://doi.org/10.1007/s42247-021-00194-6
10. A. Sehmi, H.B. Ouici, A. Guendouzi, M. Ferhat, O. Benali and F. Boudjellal, *J. Electrochem. Soc.*, **167**, 155508 (2020); https://doi.org/10.1149/1945-7111/abab25
11. D.K. Verma, Y. Dewangan, A.K. Dewangan and A. Asatkar, *J. Bio. Tribocorros.*, **7**, 15 (2021); https://doi.org/10.1007/s40735-020-00447-7
12. S. Al-Baghdadi, T.S. Gaaz, A. Al-Adili, A.A. Al-Amiery and M.S. Takriff, *Int. J. Low Carbon Technol.*, **16**, 181 (2021); https://doi.org/10.1093/ijlct/ctaa050
13. Z.P. Mathew, K. Rajan, C. Augustine, B. Joseph and S. John, *Heliyon*, **6**, e05560 (2020); https://doi.org/10.1016/j.heliyon.2020.e05560
14. S.A. Umoren and M.M. Solomon, *Open Mater. Sci. J.*, **8**, 39 (2014); https://doi.org/10.2174/1874088X01408010039
15. M.S. Goyal, S. Kumar, C. Verma, I. Bahadur, E.E. Ebenso, H. Lgaz and I.M. Chung, *J. Mol. Liq.*, **298**, 111995 (2020); https://doi.org/10.1016/j.molliq.2019.111995
16. R. Haldhar, D. Prasad, D. Kamboj, S. Kaya, O. Dagdag and L. Guo, *SN Appl. Sci.*, **3**, 25 (2021); https://doi.org/10.1007/s42452-020-04079-x
17. L. Chen, D. Lu and Y. Zhang, *Materials*, **15**, 2023 (2022); https://doi.org/10.3390/ma15062023
18. H. Assad and A. Kumar, *J. Mol. Liq.*, **344**, 117755 (2021); https://doi.org/10.1016/j.molliq.2021.117755
19. R. Solmaz, A. Salci, Y.A. Dursun and G. Kardas, *Colloids Surf. A Physicochem. Eng. Asp.*, **674**, 131908 (2023); https://doi.org/10.1016/j.colsurfa.2023.131908
20. L. Zhou, Y. Lv, Y. Hu, J. Zhao, X. Xia and X. Li, *J. Mol. Liq.*, **249**, 179 (2018); https://doi.org/10.1016/j.molliq.2017.10.129
21. A.A. Al-Amiery, A.B. Mohamad, A.A.H. Kadhum, L.M. Shaker, W.N.R.W. Isahak and M.S. Takriff, *Sci. Rep.*, **12**, 4705 (2022); https://doi.org/10.1038/s41598-022-08146-8
22. L. Tan, J. Li and X. Zeng, *Materials*, **16**, 2148 (2023); https://doi.org/10.3390/ma16062148
23. A.A.H. Al-Amiery, Y.K. Al-Majedy, A.A.H. Kadhum and A.B. Mohamad, *Molecules*, **20**, 366 (2014); https://doi.org/10.3390/molecules20010366
24. M. Abdallah, H.M. Al-Tass, B.A. AL Jahdaly and A.S. Fouda, *J. Mol. Liq.*, **216**, 590 (2016); https://doi.org/10.1016/j.molliq.2016.01.077
25. M. Goyal, S. Kumar, I. Bahadur, C. Verma and E.E. Ebenso, *J. Mol. Liq.*, **256**, 565 (2018); https://doi.org/10.1016/j.molliq.2018.02.045
26. S. Zamindar, S. Mandal, M. Murmu and P. Banerjee, *Mater. Adv.*, **5**, 4563 (2024); https://doi.org/10.1039/D4MA00156G
27. A. Upadhyay, A.K. Purohit, G. Mahakur, S. Dash and P.K. Kar, *J. Mol. Liq.*, **333**, 115960 (2021); https://doi.org/10.1016/j.molliq.2021.115960
28. H. Liu, B. Fan, Z. Liu, X. Zhao, B. Yang, X. Zheng and H. Hao, *J. Ind. Eng. Chem.*, **106**, 297 (2022); https://doi.org/10.1016/j.jiec.2021.11.004
29. S.B. Al-Baghdadi, F.G. Hashim, A.Q. Salam, T.K. Abed, T.S. Gaaz, A.A. Al-Amiery, A.A.H. Kadhum, K.S. Reda and W.K. Ahmed, *Results Phys.*, **8**, 1178 (2018); https://doi.org/10.1016/j.rinp.2018.02.007
30. F. Wang, T. Ma, S. Zhang, B. Tan, L. Guo, H. Du Lei, X. Wang, X. Han and R. Liu, *J. Mol. Liq.*, **398**, 124207 (2024); https://doi.org/10.1016/j.molliq.2024.124207
31. S.A. Al Kiey, A.A. El-Sayed and A.M. Khalil, *Colloids Surf. A: Physicochem Eng.*, **683**, 133089 (2024); https://doi.org/10.1016/j.colsurfa.2023.133089
32. A. Belkheiri, K. Dahmani, Z. Aribou, O. Kharbouch, E. Nordine, A.E.M.A. Allah, M. Galai, M.E. Touhami, M.K. Al-Sadoon, B.M. Al-Maswari and Y. Ramli, *Int. J. Electrochem. Sci.*, **19**, 100768 (2024); https://doi.org/10.1016/j.ijoes.2024.100768
33. I. Ahamad and M.A. Quraishi, *Corros. Sci.*, **51**, 2006 (2009); https://doi.org/10.1016/j.corsci.2009.05.026
34. M. Goyal, H. Vashisht, A. Kumar, S. Kumar, I. Bahadur, F. Benhiba and A. Zarrouk, *J. Mol. Liq.*, **316**, 113838 (2020); https://doi.org/10.1016/j.molliq.2020.113838
35. D.Q. Huong, T. Duong and P.C. Nam, *ACS Omega*, **4**, 14478 (2019); https://doi.org/10.1021/acsomega.9b01599
36. R. Karthikaiselvi and S. Subhashini, *Arab. J. Chem.*, **10(S1)**, S627 (2017); https://doi.org/10.1016/j.arabjc.2012.10.024
37. O.A. Hazazi, M. Abdallah and E.A.M. Gad, *Int. J. Electrochem. Sci.*, **9**, 2237 (2014); https://doi.org/10.1016/S1452-3981(23)07923-3
38. A. Boutouil, M.R. Laamari, I. Elazhary, H. Anane, A.B. Tama and S. Stiriba, *Anti-Corros. Methods Mater.*, **66**, 544 (2019); https://doi.org/10.1108/ACMM-01-2019-2055
39. I.A.A. Aziz, M.H. Abdulkareem, I.A. Annon, M.M. Hanoon, M.H.H. Al-Kaabi, L.M. Shaker, A.A. Alamiery, W.N.R.W. Isahak and M.S. Takriff, *Lubricants*, **10**, (2022); https://doi.org/10.3390/lubricants10020023
40. A. Hamdy and N.Sh. El-Gendy, *Egypt. J. Pet.*, **22**, 17 (2013); https://doi.org/10.1016/j.ejpe.2012.06.002
41. G. Quartarone, L. Bonaldo and C. Tortato, *Appl. Surf. Sci.*, **252**, 8251 (2006); https://doi.org/10.1016/j.apsusc.2005.10.051
42. R.T. Loto, C.A. Loto, O. Joseph and G. Olanrewaju, *Results Phys.*, **6**, 305 (2016); https://doi.org/10.1016/j.rinp.2016.05.013
43. V.R. Palayoor, J.T. Kakkassery, S.S. Kanimangalath and S. Varghese, *Int. J. Ind. Chem.*, **8**, 49 (2017); https://doi.org/10.1007/s40090-016-0101-0
44. P.L. Sophie and N. Antony, *J. Emerg. Technol. Innov. Res.*, **6**, 217 (2019).
45. A.F.S. Abdul Rahiman and S. Sethumanickam, *Arab. J. Chem.*, **10**, S3358 (2017); https://doi.org/10.1016/j.arabjc.2014.01.016
46. R. Karthikaiselvi and S. Subhashini, *J. Assoc. Arab Univ. Basic Appl. Sci.*, **16**, 74 (2014); https://doi.org/10.1016/j.jaubas.2013.06.002
47. A.F.S. Abdul Rahiman and S. Sethumanickam, *Arab. J. Chem.*, **10**, S3358 (2017); https://doi.org/10.1016/j.arabjc.2014.01.016
48. O.A. Akinbulumo, O.J. Odejobi and E.L. Odekanle, *Results Mater.*, **5**, 100074 (2020); https://doi.org/10.1016/j.rinma.2020.100074
49. N. El Hamdani, R. Fdil, M. Tourabi, C. Jama and F. Bentiss, *Appl. Surf. Sci.*, **357A**, 1294 (2015); https://doi.org/10.1016/j.apsusc.2015.09.159
50. S. Yadav, S. Kaushik, N. Dheer, S. Kumar, G. Singh, M. Chaudhary and M. Gupta, *J. Appl. Nat. Sci.*, **15**, 1315 (2023); https://doi.org/10.31018/jans.v15i3.4969
51. A.M. Abuelela, M.A. Bedair, E.S. Gad, Y.F. El-Aryan, W.A.A. Arafa, A.K. Mourad, H. Nady and S. Eid, *Sci. Rep.*, **14**, 13310 (2024); https://doi.org/10.1038/s41598-024-64199-x
52. M.A.M. El-Haddad, A. Bahgat Radwan, M.H. Sliem, W.M.I. Hassan and A.M. Abdullah, *Sci. Rep.*, **9**, 3695 (2019); https://doi.org/10.1038/s41598-019-40149-w

53. N. Betti, A.A. Al-Amiery and W.K. Al-Azzawi, *Molecules*, **27**, 6254 (2022); https://doi.org/10.3390/molecules27196254
54. H.B. Fan, C.Y. Fu, H.L. Wang, X.P. Guo and J.S. Zheng, *Br. Corros. J.*, **37**, 122 (2002); https://doi.org/10.1179/000705902225004383
55. S. Kumar, M. Goyal, H. Vashisht, V. Sharma, I. Bahadur and E.E. Ebenso, *RSC Adv.*, **7**, 31907 (2017); https://doi.org/10.1039/C6RA27526E
56. M.E. Belghiti, S. Bouazama, S. Echihi, A. Mahsoune, A. Elmelouky, A. Dafali, K.M. Emran, B. Hammouti and M. Tabyaoui, *Arab. J. Chem.*, **13**, 1499 (2020); https://doi.org/10.1016/j.arabjc.2017.12.003
57. H. Musa, U. Bishir, I.M. Adamu and I.M. Bashir, *Res. J. Chem. Environ.*, **24**, 99 (2020).
58. N. Idlahoussaine, M. Lasri, R. Idouhli, W. Daoudi, B. EL Ibrahimi, E. Berdimurodov, M. El Ouardi, A. AIT Addi, N. Aliev, A. EL Aatiaoui and A. Abouelfida, *J. Mol. Struct.*, **1305**, 137705 (2024); https://doi.org/10.1016/j.molstruc.2024.137705
59. N. Haldar, H.S. Shukla and G. Udaybhanu, *Asian J. Chem.*, **23**, 5127 (2011).
60. H.H. Hammud, N.S. Sheikh, I. Shawish, H.A. Bukhamsin, D.E. Al-Hudairi, A.L.X. Wee, M.H.S.A. Hamid, S.A. Maache, H.H. Al-Rasheed, A. Barakat, A. El-Faham and H.M. Abd El-Lateef, *R. Soc. Open Sci.*, **11**, 231229 (2024); https://doi.org/10.1098/rsos.231229
61. M. Gupta, K. Bhrara and G. Singh, *Corros. Prot. Mater.*, **31**, 17 (2012).
62. N.N. Hau and D.Q. Huong, *J. Mol. Struct.*, **1277**, 134884 (2023); https://doi.org/10.1016/j.molstruc.2022.134884